Boundary Conditions and Fast Algorithms For Surface Reconstructions from Synthetic Aperture Radar Data

Daniel N. Ostrov
Department of Mathematics
Santa Clara University
Santa Clara, CA 95053

October 26, 1995

Abstract

Most attempts to determine surface height from noiseless Synthetic Aperture Radar (SAR) data involve approximating the surface by solving a related standard Shape From Shading (SFS) problem. Through analysis of the underlying partial differential equations for both the original SAR problem and the approximating standard SFS problem we demonstrate significant differences between them. For example, if it is known that the surface is smooth, the standard SFS problem can generally be uniquely solved from knowledge of the height and concavity at one surface point, whereas for SAR, multiple valid solutions will generally exist unless height information is specified along entire curves on the surface (i.e., boundary conditions). Unlike the standard SFS approximation, the underlying SAR equation can be re-expressed as a time-dependent Hamilton-Jacobi equation. This transformation allows us to compute the correct surface topography from noiseless SAR data with boundary conditions extremely quickly. Finally, we consider the effect of radar noise on the computed surface reconstruction and discuss the ability of the presented PDE method to quickly compute an initial surface that will significantly cut the computational time needed by cost minimization algorithms to approximate surfaces from noisy radar data.

1 Introduction

One of the primary goals of image and radar analysis is to reconstruct 3-D topographical maps from 2-D intensity data. This is generally referred to as the Shape From Shading (SFS) problem. The standard SFS problem involves optical intensity data that is specified in Cartesian coordinates on a plane perpendicular to the direction traveled by light rays emanating from a single light source. (It is useful to think of a standard black and white photograph taken by a camera employing a flash as an example). By way of contrast with the optical problem, radar data is usually collected using Synthetic Aperture Radar (SAR) which specifies the radar data in cylindrical coordinates. Unlike the standard Shape From Shading problem, the 2-D SAR intensity data has a radial coordinate which corresponds to distance in the direction traveled by the radar signal. A prominent example of the use of SAR is the 1990 Magellan Space Probe, which collected a vast amount of high resolution SAR data from the surface of Venus. One of the mission objectives of the Magellan project was to determine Venus's topography using this SAR data [1].

While the standard Shape From Shading problem has had much research devoted to it, the same cannot be said of SAR despite its common use. It is often assumed that the surface being analyzed by SAR is essentially flat, which allows the SAR SFS problem to be approximated by a corresponding standard SFS problem. It is an oversimplification, however, to treat the two SFS problems as the same, as they have significantly different physical restrictions.

There has been much progress recently in resolving the issue of uniqueness for the standard Shape From Shading problem. For typical 2-D intensity data, it is now known that a unique 3-D reconstruction can be obtained from concavity and height information for a single local maximum or local minimum on the surface.

The question immediately arises as to whether a unique 3-D reconstruction for SAR data also can follow from information from a single location on the surface. It turns out that for meaningful SAR intensity data, the answer is no. We will show that physical restrictions on SAR data show that the "local maximums" and "local minimums" that exist in standard SFS have no SAR analogue. To recover uniqueness for SAR data reconstructions, we will examine the need for appropriate boundary conditions, i.e., knowledge of the surface height along part of the 1-D boundary surrounding the 2-D region where we wish to determine the surface height. When knowledge at a local extremum is not exploited, most standard SFS problems require boundary conditions along the entire 1-D boundary surrounding the 2-D region of interest. For the SAR problem, we will show that we require the height only along a subsection of this boundary.

Although the above conclusions will hold for non-Lambertian surface data (such as the Magellan data from Venus), this paper will focus its analysis on the standard SFS partial differential equation for a Lambertian surface, which relates the unknown surface height,

$Z(x, y)$, to the known radar intensity data, $I(x, y)$, through the equation

$$I(x, y) = \frac{1}{\sqrt{1 + Z_x^2 + Z_y^2}}, \tag{1}$$

and also on the SAR SFS partial differential equation for a Lambertian surface, which relates the "angular surface height", $u(r, y)$, to the radar intensity data, $I(r, y)$, through

$$I(r, y) = \frac{u_r^2}{\sqrt{1 + u_r^2 + u_y^2}}. \tag{2}$$

The above equations both have the property that knowledge about the solution at a single location in the (x, y) (or (r, y)) plane propagates along a specific curve in the plane. These curves are called *characteristics*. Specifically, knowledge of the height and the partial derivatives of the height function at one location on a characteristic curve leads to knowledge of the height (and the partial derivatives of the height function) at all locations on the curve. Combining the behavior of these characteristic curves with physical restrictions on the radar intensity data will allow us to determine the minimum amount of information needed to solve eqs (1) and (2) (i.e., the minimum amount of information needed to determine the topology of the surface).

For the SAR equation, there will be an additional benefit from the analysis of its characteristics. We will show that the nature of information propagation in the SAR equation is mathematically the same as the propagation of information inherent in hyperbolic equations that describe time-dependent physical phenomena such as fluid flow. This will suggest a transformation of eq (2) into the form

$$u_r + f(I(r, y), u_y) = 0, \tag{2a}$$

where

$$f(I, u_y) = -I\sqrt{.5 + \sqrt{.25 + (1 + u_y^2)/I^2}}.$$

Eq (2a) is a time dependent *Hamilton-Jacobi equation*. There are fast numerical methods that can be employed to compute the solution of time dependent Hamilton-Jacobi equations with high order accuracy. For example, we will employ a 3rd order accurate finite difference scheme to solve eq (2a), which has significant advantages over the control theory based methods that are appropriate for computing the solution of standard SFS problems.

The organization of this paper is as follows: In the next section, we will explore the history and recent developments in standard SFS problems and see how they have been applied in SAR SFS problems. In the third section we will derive the two SFS partial differential equations given in eq (1) and eq (2) and discuss the relevant physical constraints on the equations. In section four, we will look at the equations of the characteristic curves for eq (1) and eq (2) and consider the differences in the nature of the two sets of characteristics.

This will lead to a discussion of the appropriate boundary conditions for solving the two partial differential equations. In section five, we will transform the SAR SFS equation into its Hamilton-Jacobi form and examine the advantages of exploiting the finite element methods available for Hamilton-Jacobi equations which cannot be employed on standard SFS problems. Finally, in section six, we will consider the effect of the noise inherent in SAR intensity data on the accuracy of the reconstruction and examine the benefits of using finite element methods as a preprocessor for existing cost minimization algorithms.

2 History of Standard and SAR Shape From Shading Methods

In 1951 van Diggelen considered the process of using photographic images of the moon (i.e., the brightness of the moon's surface) to determine information about the moon's topography [2]. His paper was the starting point for two separate, but parallel, branches of research.

One branch continued to explore the topography of moons and planets. The process, which was referred to as "photogrammetry" and later "photoclinometry" in the literature, was further investigated in the 1960s by Rindfleisch [3], Watson [4], and others. When the photographic images of the planets and moons were replaced by superior radar images, the field, appropriately, altered its name to "radarclinometry". The other branch of research applied van Diggelen's ideas to questions arising in the field of computer vision. The computer vision literature, however, used the term "Shape From Shading" to describe this process. The two areas remained basically unaware of each other until 1987.

In the 1980s Robert Wildey wrote a series of papers on radarclinometry using SAR data. In 1986 Wildey [5] approximated SAR radar behavior with the equation for radar in Cartesian coordinates (eq (1)) by assuming that the planetary surface of interest was "approximately planar". The paper's method of solving eq (1) with SAR data required "one dimensional ground truth" (i.e., boundary conditions for the equation).

After this paper, Wildey discussed his radarclinometry work with B. K. P. Horn, the author a number of important works in Shape From Shading. Horn had analyzed eq (1) using characteristic curves in 1975 [6], and, in fact, had looked at creating a computer solution to eq (1) based strictly on characteristic curves.

After his discussions with Horn, Wildey, in a 1987 paper [7], presented a non-characteristic curve based surface integral approach to SAR data that requires a boundary condition. Unfortunately, the equations and numerical methods used by Wildey lead to numerical instablities. This, combined with Wildey's concern that his numerical scheme may try to propagate the solution in a direction perpendicular to the characteristic curves (which, from his conversations with Horn, he correctly notes cannot succeed), leads him to abandon his approach as "holding little promise." Wildey also mentions efforts by Frankot and Chellappa to remove the necessity of boundary conditions to solve eq (1) and eq (2), which he characterizes as

"promising".

Frankot and Chellappa's work evolved from methods developed by Horn to analyze the standard SFS problem. After Horn abandoned his characteristic strip approach, he and others developed methods based on Calculus of Variations to determine $p = Z_x$ and $q = Z_y$ in eq (1) [8, 9, 10]. This method determines p and q by minimizing a cost functional based on fidelity to the intensity data, I, and a smoothness constraint (since wildly varying surfaces are unlikely). This method is particularly attractive because it can compensate for the noise that is inherent in real intensity data. In 1987, Frankot and Chellappa further improved this approach by requiring that the p and q determined by the cost minimization correspond to a real (integrable) surface, Z, which is accomplished by requiring that the mixed partials p_y and q_x be equal [11]. Chellappa and others expanded upon this method in [12, 13, 14].

To solve eq (1), Horn's algorithms utilized boundary conditions; specifically knowledge of the height of the surface along the 1-D path surrounding the region of interest. Frankot and Chellappa's algorithm did not employ boundary conditions. Instead it utilized a priori knowledge of the low frequency Fourier modes of the solution. This leads to an approximation of the boundary condition and therefore will lead to inaccuracies in the surface reconstruction even in the absence of noise. The Fourier method was employed for two reasons: 1) The algorithm was intended to be applied to noisy intensity data, so it is reasonable to use an approximate boundary condition since the surface can only be approximated from noisy data, and 2) When applied to eq (2), the algorithm was intended to exploit the low resolution altimetry data that Magellan collected in addition to the SAR data. Unfortunately, Magellan's altimetry data is of such low resolution that it does not provide much information concerning the low Fourier modes. This lack of low frequency information will allow the algorithm to generate a wide range of solutions that will still conform to the partial differential equation, but will be progressively inaccurate since a lack of low frequency information allows for further deviation from the true boundary condition.

When Frankot and Chellappa presented the application of their method to Synthetic Aperture Radar data in 1987 [15] and 1990 [16], they thoroughly described a number of models for SAR data. Whereas eq (1) describes intensity data gathered from a Lambertian surface in Cartesian (rectangular) coordinates, Frankot and Chellappa point out that eq (2) is the appropriate equation for describing intensity data gathered from a Lambertian surface in the cylindrical coordinate system employed by SAR. Since the assumption that the surface is Lambertian (i.e., that the surface scatters radar waves equally in all directions) is poor for the large radar wavelengths employed by the Magellan Space Probe's SAR system, Frankot and Chellappa looked at the empirical equations for non-Lambertian surfaces, as well. They found that the generalized Lambert model

$$I(r, y) = \left(\frac{u_r}{\sqrt{1 + u_r^2 + u_y^2}} \right)^k u_r \tag{3}$$

worked best for Magellan data. When $k = 1$ in eq (3), we recover eq (2), the Lambertian

case; for Magellan data, Frankot and Chellappa found that larger values of k were more appropriate. They applied their minimization scheme to eq (3) to estimate the Venusian topographical map.

Because cost minimization produces reasonably smooth topographical maps even when the SAR data is noisy, subsequent attempts to solve eq (2) and eq (3) when the intensity data is noisy have relied on modifications of Frankot and Chellappa's algorithm [17] or closely related ideas like Bayesian estimation [18].

Much is known about the conditions under which a unique solution to eq (1) exists. Local uniqueness and existence results around critical points (i.e., (x, y) locations where $I(x, y) = 1$ and therefore $\nabla Z = 0$) were determined by Horn in the 1970s and Bruss in 1982 [19] and Saxberg in 1992 [20]. More recently, Dupuis and Oliensis have proven [21, 22, 23] that intensity data for any smooth (twice differentiable), non-self-occluding surface with a finite number of critical points corresponds to a unique surface if we know the surface height Z of one of the critical points and whether that critical point corresponds to a local maximum or a local minimum of the surface. In other words, from knowledge about one point on the surface, we can uniquely establish (for a large class of surfaces) the entire surface; we only require boundary conditions at points where neither the positive nor the negative trajectory of the surface gradient flow field through the boundary point converges to any critical point. Further, [21] also establishes a convergent control theory based algorithm to compute this solution. Even more recently, Eastwood [24] has presented a simple flow field argument that estabishes a global uniqueness result that is only slightly less generalthan Dupuis and Oliensis's.

In this paper we will explore the boundary conditions that, unlike the standard SFS case, are necessary in the SAR case to uniquely determine surface topography. Without these conditions the noiseless data will correspond to a wide range of possible solutions. Further, we will present a stable numerical scheme for SAR equations that never attempts to propagate the solution in a direction perpendicular to the characteristics. To show this, we begin by deriving both the standard and SAR Shape From Shading equations in the next section.

For further information on the history of Shape From Shading and Radarclinometry, we direct the reader to Hurt's overview of the field [25].

3 Derivation of Standard and SAR Shape From Shading Equations

We begin this section by reviewing the derivation of the standard Shape From Shading equation, which we then connect to the derivation of the Synthetic Aperture Radar Shape From Shading equation. While we exploit, as much as possible, the similarities between these two derivations, we will also encounter physical differences that create significant contrasts

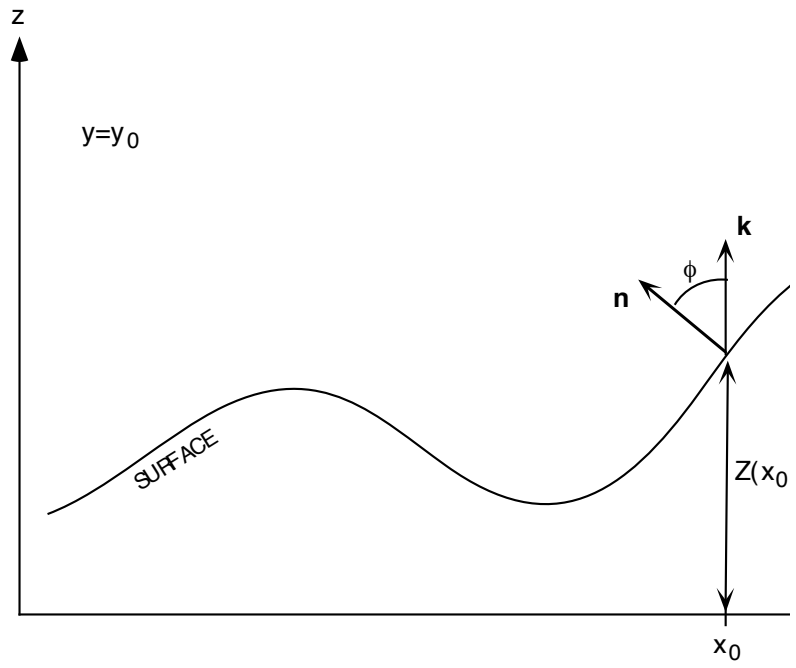

Figure 1: *Surface for a standard shape from shading problem. ϕ is the angle between the surface normal and the vertical direction. $Z(x, y)$ is the height of the surface.*

in the two solutions' behaviors.

The standard Shape From Shading equation follows from a very simple physical model for a light source placed above a surface along with a camera that records the light intensity of the illuminated surface. (It is useful to think about a camera equipped with a flash and black and white film taking shots looking directly downward onto a surface.) Assume the light coming directly down onto the surface has a uniform brightness so the power per unit area of flat surface, P_s, is constant (i.e., the time-averaged magnitude of the Poynting vector equals P_s). The incident power per unit area of actual surface, P_i, is related to P_s by

$$P_i = P_s \cos(\phi), \tag{4}$$

where ϕ is the angle between the unit surface normal, $\mathbf{n}$, and the unit vector pointing up toward the light source, $\mathbf{k}$ (see fig. 1).

If $Z(x, y)$ is the surface height corresponding to an (x, y) location, then we can express

the unit surface normal in terms of the partial derivatives of Z:

$$\mathbf{n} = \frac{-Z_x\mathbf{i} - Z_y\mathbf{j} + \mathbf{k}}{\sqrt{1 + Z_x^2 + Z_y^2}}, \tag{5}$$

and since $\cos(\phi) = \mathbf{n} \cdot \mathbf{k}$, eq (4) can be reexpressed as:

$$P_i = \frac{P_s}{\sqrt{1 + Z_x^2 + Z_y^2}}. \tag{6}$$

We now consider the amount of power returned to the camera. For the returned data to have any meaning, we must know the surface albedo function. The albedo, which is defined as the ratio of power emitted by the surface at the wavelength(s) of the incident light to power incident on the surface, is a measure of how "white" the surface is. As long as the albedo function is known (which, unfortunately, is often not the case), it is easily accommodated; for the sake of simplicity we will set the albedo to be equal to 1.

We also use the assumption that the surface is Lambertian here. Since a Lambertian surface scatters light waves equally in all directions, the power returned to the camera, P_r, is proportional to the power incident per area on the surface. (So $P_r = k_1 P_i$ where k_1 is a constant). Combining this with eq (6) leads to the standard Shape From Shading equation:

$$I(x, y) = \frac{1}{\sqrt{1 + Z_x^2 + Z_y^2}}, \tag{1}$$

where $I(x, y)$, the intensity, which is defined as $P_r/(k_1 P_s)$, is determined by the returned radar signal.

Before we move on to the SAR case, we note that it is assumed in the above analysis that the camera collects the data in rectangular coordinates. In other words, cameras (and satellites and eyes) collect data in pixels. We are assuming above that the "pixel" corresponds to a small fixed amount of area in the (x, y) plane. So, in fact, for a given pixel point, (x_i, y_j), and pixel area, $\Delta x \Delta y$, we actually have

$$P_r(x_i, y_j) = k_2 \int_{x_i - \frac{\Delta x}{2}}^{x_i + \frac{\Delta x}{2}} \int_{y_j - \frac{\Delta y}{2}}^{y_j + \frac{\Delta y}{2}} P_i(x, y)\, dydx. \tag{7}$$

We approximate eq (7) by $P_r(x_i, y_j) \doteq k_2 P_i(x_i, y_j) \Delta x \Delta y$, which leads to

$$I(x_i, y_j) \equiv \frac{P_r(x_i, y_j)}{k_2 P_s \Delta x \Delta y} = \frac{1}{\sqrt{1 + Z_x^2(x_i, y_j) + Z_y^2(x_i, y_j)}} \tag{8}$$

and eq (1), of course, is just the continuous analogue of eq (8).

In the case of SAR, we have a satellite that moves above a surface in the y direction. The radar signal sent from the satellite is at an angle, φ, with the vertical direction (see

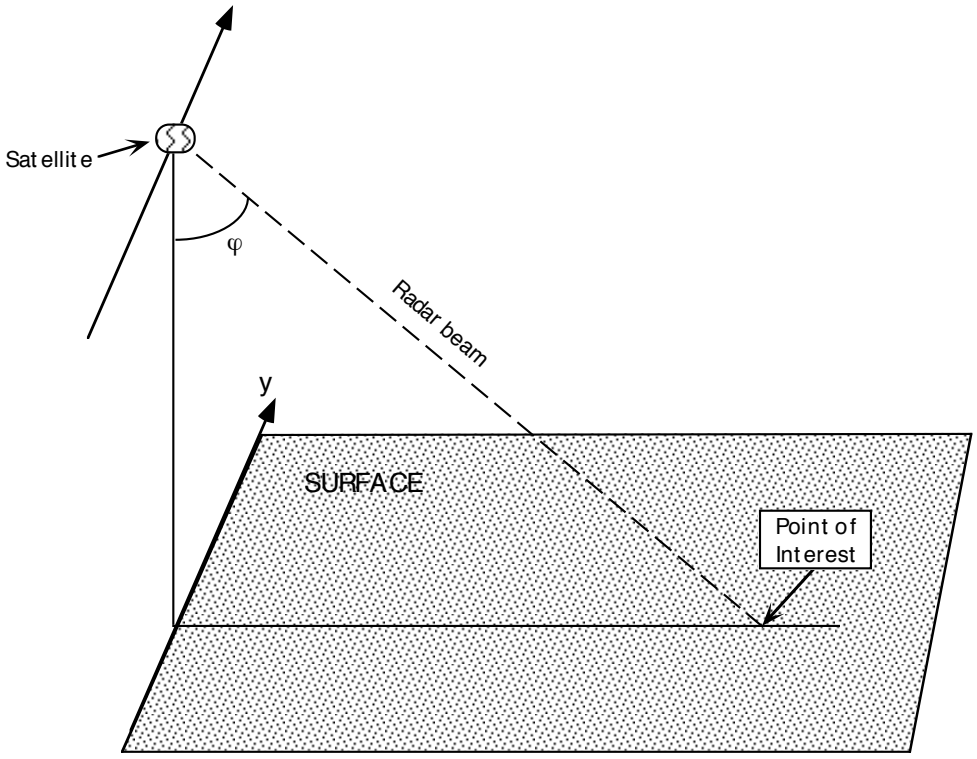

Figure 2: *Satellite transmission of Synthetic Aperture Radar signals. The satellite moves parallel to the ground in the y direction. The radar signal is sent perpendicular to the y direction at an angle φ with the vertical direction.*

fig. 2). In practice φ is essentially constant since the satellite is far from the surface. We can express the plane perpendicular to the y direction in two useful coordinate systems. The first coordinate system is Cartesian. In order to make a comparison with the standard SFS case we consider z to be in the direction of the radar beam and x to be perpendicular to z and y. The second coordinate system is polar. Consider r to be the radial distance in the (x, z) plane from the satellite and θ to be the angle from an arbitrary reference line chosen for $\theta = 0$. In synthetic aperture radar, the processed, filtered radar data is expressed in $\Delta r \Delta y$ pixels. This is essentially a ramification of the fact that for a fixed value of y, the amount of time for the radar beam to leave and return to the satellite is strictly a function of r. (One might wonder why the data isn't in spherical coordinates since the radar beam spreads in the $\pm y$ directions as well as in the (r, θ) plane. The data is in cylindrical coordinates because it is collected at a number of different y locations – which, during processing and filtering, allows the y component of the radar to be isolated and, basically, removed.)

To express the SAR data in the Cartesian coordinate system, it is necessary to make an assumption about the surface so that the $\Delta r \Delta y$ pixels can be approximated by $\Delta x \Delta y$

pixels. The assumption made is that the surface is essentially flat. If this assumption holds, the approximation

$$\Delta r \doteq \Delta x \tan\varphi, \tag{9a}$$

which implies

$$r_i \doteq r_0 + (x_i - x_0)\tan\varphi, \tag{9b}$$

can be made. With this approximation, which was made by Wildey in all of his work, the SAR data is thought of as standard SFS data, and the surface height, $Z(x, y)$, is then described by the standard SFS equation, eq (1). (Although Wildey's work employed other approximations that led to a 2nd order PDE.)

This flat surface approximation, however, is often poor. For surfaces with small hills and valleys, the approximation causes a distortion of the reconstructed surface. The parts of the surface that are closer to being perpendicular to the radar signal tend to be shrunk in the reconstruction and the parts of the surface that are more parallel to the radar signal become elongated. The approximation is a disaster when we have a surface where the hills and valleys are so large that a part of the surface becomes perpendicular to the radar signal. When this happens, it is almost certain that there will be two (or more) locations on the surface in the (x, z) plane that are equally distant from the satellite (see fig. 3). (It is uncertain only when the location where the surface is perpendicular corresponds to a saddle point of $Z(\cdot, y)$; since saddle points are extremely improbable in practice we disregard this singular case.) Since the returned radar signal comes from two spatial locations, we encounter "layover" in the data, which means the SAR data exhibits double images and reconstructions become impractical. Note that the surface is perpendicular to the signal when ϕ, the angle between the surface normal and the radar beam, equals 0.

We now wish to derive eq (2), which will express the SAR SFS equation in the appropriate cylindrical coordinate reference frame, allowing us to avoid the distorting effects caused by the approximation in (9). Since the intensity data is expressed in (r, y) coordinates, we need to express the surface in terms of θ. We define $u(r, y) = r_0\Theta(r, y)$, where $\Theta(r, y)$ is the θ coordinate of a surface location whose other two coordinates are r and y, and r_0 is the average distance between the satellite and the surface. Because, in practice, the distance between the satellite and the surface is much larger than the range of r values in the data, $r \doteq r_0$, and we can think of $u(r, y)$ as the length of the arc, for fixed r and y, that connects the surface to the reference plane $\theta = 0$ (see fig. 4).

As in the standard SFS case, eq (4), which relates the power of the radar signal, P_s, to the power incident on the surface, P_i, still holds:

$$P_i = P_s \cos(\phi), \tag{4}$$

but we now must express $\cos(\phi)$ in terms of u as opposed to Z:

$$\cos(\phi) = \frac{u_r}{\sqrt{1 + u_r^2 + u_y^2}} \tag{10}$$

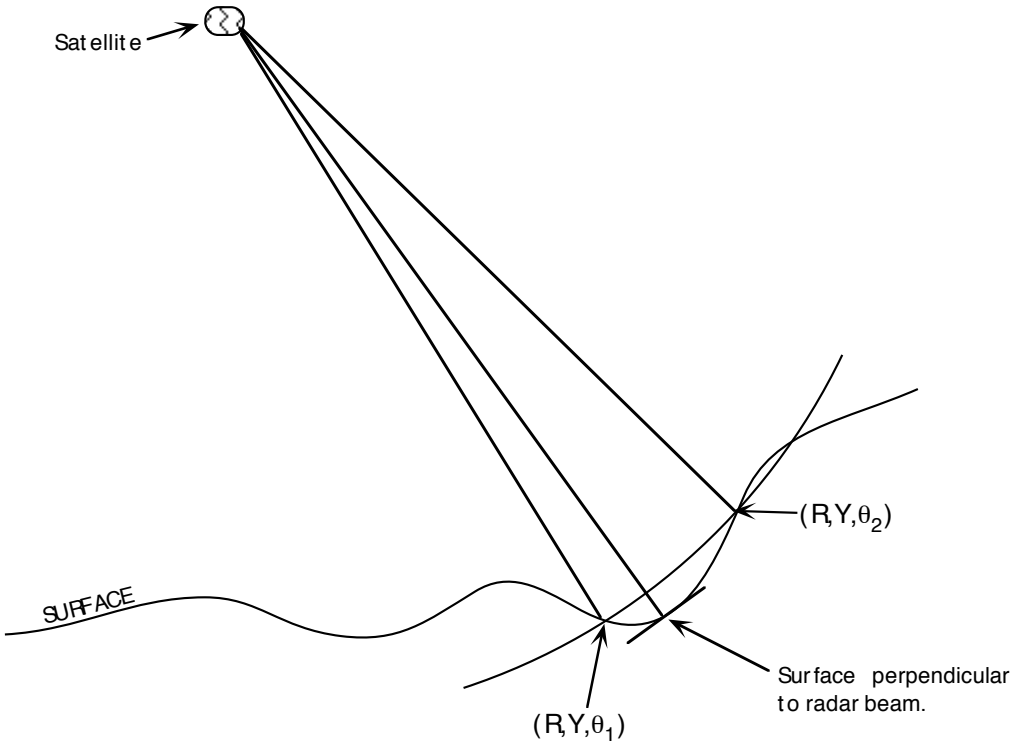

Figure 3: *Layover in SAR data collection. The surface shown represents the cross-section where $y = Y$, a constant. When there is any location on the surface that is perpendicular to the radar beam, it is (almost always) indicative of regions surrounding the point where a given value of r (e.g., $r = R$ in the figure) corresponds to two locations on the surface, which leads to intensity data that appear to contain "double exposures".*

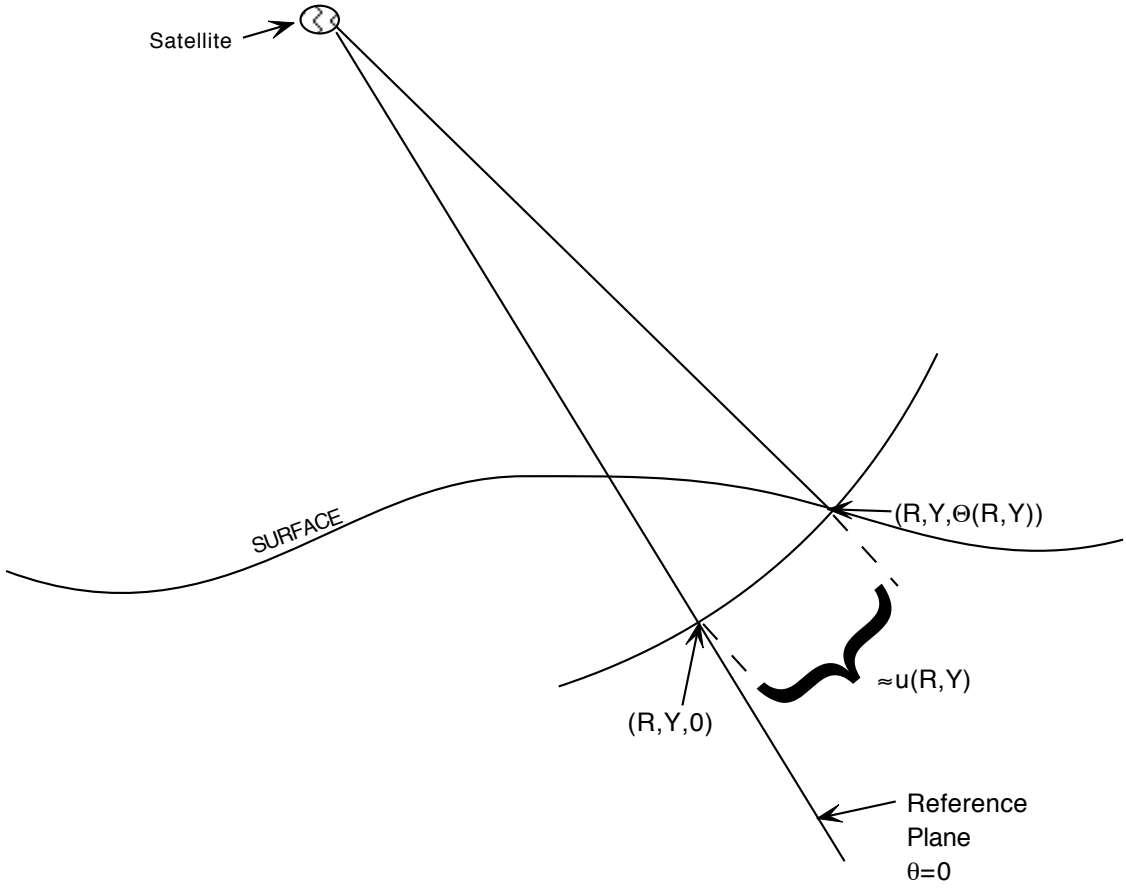

Figure 4: *Meaning of $u(r, y)$. We consider the cross-section of the surface where $y = Y$. Since r varies only a small amount over the range of collected intensity data, we can think of $u(R, Y)$ as the arclength of the subsection of the circle of radius R centered at the satellite that lies between the reference plane $\Theta = 0$ and the surface.*

For a Lambertian surface with a unit albedo, the power returned to the satellite, P_r, was related to P_i in the standard SFS case by $P_r(x_i, y_j) \doteq k_2 P_i(x_i, y_j)\Delta x \Delta y$. This translates in the polar case to $P_r(r_i, y_j) \doteq k_2 P_i(r_i, y_j)\Delta u \Delta y$, which, in terms of Δr and Δy, is approximately

$$P_r(r_i, y_j) \doteq k_2 P_i(r_i, y_j) u_r(r_i, y_j)\Delta r \Delta y. \tag{11}$$

Combining eqs (4), (10), and (11) yields

$$I(r_i, y_j) \equiv \frac{P_r}{k_2 P_s \Delta r \Delta y} = \frac{u_r^2(r_i, y_j)}{\sqrt{1 + u_r^2(r_i, y_j) + u_y^2(r_i, y_j)}}, \tag{12}$$

and the continuous analogue of eq (12) is eq (2):

$$I(r, y) = \frac{u_r^2}{\sqrt{1 + u_r^2 + u_y^2}}. \tag{2}$$

The non-Lambertian case is slightly more complex. The relationship between P_r and P_i can be expressed by eq (11) or by

$$P_r \doteq k_2 P_i \cos(\phi)\Delta S \tag{13}$$

where ΔS, which represents a small amount of the actual surface area, can be expressed as $\Delta S \doteq \sqrt{1 + u_r^2 + u_y^2}\Delta r \Delta y$. When the surface is not Lambertian, the $\cos(\phi)$ term in eq (13) can be modeled by $\cos^k(\phi)$, where k becomes larger as the surface becomes more reflective (mirrorlike). Combining this with eqs (4) and (10) yields eq (3):

$$I(r, y) = \left(\frac{u_r}{\sqrt{1 + u_r^2 + u_y^2}}\right)^k u_r, \tag{3}$$

where $k \geq 1$.

We wish to note some physical restrictions on the variables in eq (2) (and eq (3)), which will have significant ramifications on our analysis. Since we cannot use SAR data tainted by layover, u_r and I cannot become infinitely large and $\phi \neq 0$. More importantly, we cannot use data that contains "holes" (in other words (r, y) values that do not have intensity values associated with them). Physically, this occurs when the surface occludes itself causing radar "shadows" for the occluded region of the surface. Mathematically, this will occur — barring singular cases — if $u_r = 0$ or $u_y = \infty$. Therefore, we require that u_r is never equal to zero and that $u_y \neq \infty$ (which also implies that $I(r, y) \neq 0$ and $\phi \neq \frac{\pi}{2}$).

4 Characteristic Curves for Shape From Shading Equations

Both eqs (1) and (2) can be expressed in the form

$$F(u_{\xi_1}, u_{\xi_2}, I(\xi_1, \xi_2)) = 0, \tag{14}$$

where u represents the unknown function (i.e., Z in eq (1), u in eq (2)), I is the intensity, and ξ_1 and ξ_2 represent the spatial variables (i.e., x and y in eq (1), r and y in eq (2)).

As with any first order PDE, information concerning the solution only propagates in the (ξ_1, ξ_2) plane along characteristic curves, which we will parameterize by s. We define $\Xi_i(s)$ (where $i = 1$ or 2) to be the value of ξ_i on the characteristic at s, and we define $U(s)$ and $U_{\xi_i}(s)$ to represent $u(\Xi_1(s), \Xi_2(s))$ and $u_{\xi_i}(\Xi_1(s), \Xi_2(s))$ respectively. The characteristic equations are

$$\frac{d\Xi_i}{ds}(s) = \frac{\partial F}{\partial u_{\xi_i}}(U_{\xi_1}(s), U_{\xi_2}(s), I(\Xi_1(s), \Xi_2(s))) \qquad i = 1, 2, \tag{15}$$

$$\frac{dU}{ds} = \sum_{j=1}^{2} U_{\xi_j} \frac{dF}{du_{\xi_j}}, \qquad \text{and} \tag{16a}$$

$$\frac{dU_{\xi_i}}{ds} = -\frac{\partial F}{\partial I}\frac{\partial I}{\partial \xi_i} \qquad i = 1, 2. \tag{16b}$$

We first consider the characteristics for eq (1), the standard SFS equation. Assuming that $I(x, y)$ is nonzero (which is a minor assumption since $I = 0$ implies — with probability equal to one — that the surface function, $Z(x, y)$, is discontinuous and therefore beyond our analysis here), we can algebraically rearrange eq (1):

$$F(Z_x, Z_y, I(x, y)) = \frac{1}{2}(1 + Z_x^2 + Z_y^2) - \frac{1}{2I^2} = 0. \tag{17}$$

Next we apply eq (15) to eq (17):

$$\frac{dX}{ds} = Z_x(X(s), Y(s)) \tag{18a}$$

$$\frac{dY}{ds} = Z_y(X(s), Y(s)), \tag{18b}$$

where $X(s)$ and $Y(s)$, which correspond to $\Xi_1(s)$ and $\Xi_2(s)$ in eq (15), are the values of x and y respectively on the characteristic. From eq (18) it is clear that the characteristic path progresses in the direction of the gradient of Z.

The uniqueness of Z for C^2 (i.e., twice continuously differentiable) surfaces with a finite number of critical points (that is, points where $I = 1$) follows from the fact that characteristic curves converge to the critical points that correspond to local minima and maxima of the surface.

This connection between a local extremum and all of the points surrounding the extremum can be exploited to show that knowledge of Z at an extremum — combined with knowledge of whether the extremum is a minimum or a maximum — leads to knowledge of Z for all the points surrounding the extremum, including some of the other critical points near the extremum. Knowledge of Z for any of the surrounding critical points leads to knowledge of Z for the regions surrounding the new critical points, and this process can be continued

until the solution, Z, to eq (1) is known. A proof of this process, based on control theory, can be found in [21].

The solution of the standard SFS equation from knowledge at one maximum or minimum of the surface suggests that it may be possible to also solve the related SAR SFS equation from knowledge at one point. Unfortunately, this is not the case, as we see in the following analysis of the SAR equation's characteristics.

Eq (2) can be algebraically rearranged into the form

$$F(u_r, u_y, I(r,y)) = u_r^4 - I^2(1 + u_r^2 + u_y^2) = 0. \tag{19}$$

As before, we determine the differential equations defining a characteristic path by applying eq (15) to eq (19):

$$\frac{dR}{ds} = 4u_r^3 - 2I^2 u_r \tag{20a}$$

$$\frac{dY}{ds} = -2I^2 u_y. \tag{20b}$$

where $R(s)$ and $Y(s)$ are the values of r and y respectively on the characteristic.

Again, we assume that $u(r,y)$ is a C^2 function, which implies that I must also be a C^1 function, therefore eq (20) defines a flow. Since trajectories in a flow field can only meet at critical points of the flow (i.e., locations where $\frac{dR}{ds} = \frac{dY}{ds} = 0$), we require at least one critical point if we hope to be able to determine u from knowledge at a single location. Since we can use eq (2) to quickly establish that $4u_r^2 - 2I^2 > 0$, a critical point can only occur when $u_r = 0$, but, as noted before, physically we cannot have that $u_r = 0$, since it implies — with probablility equal to 1 — that the data is unusable. (Specifically, we have holes in the intensity data, that is, regions in the (r,y) plane for which I is undefined so u cannot be determined.) Therefore, it is impossible for $u(r,y)$ to be uniquely specified from knowledge at one (r,y) location, and any method that attempts to reconstuct a surface from such information will (barring bizzare coincidence) produce a solution that does not correspond to the actual surface.

This leaves us with the question of determining the minimum amount of knowledge necessary to be able to solve eq (2). Since we will need to have information at one point on each characteristic, we begin by looking at the nature of the characteristics.

Since u_r is continuous and cannot be zero, it must always be negative or always positive. Without loss of generality, we can assume that $\varphi > 0$, which means that u_r is positive. Further, since u_r is a continuous function, and we are interested in its value on a closed, bounded region in the (r,y) plane, which we label Q, there must exist a constant K such that $u_r \geq K > 0$ over all of Q. This implies that the right hand side of eq (20a) is always greater than $2K^3$, therefore

$$\frac{dR}{ds} > 2K^3 > 0. \tag{21}$$

The inequality in (21) reveals significant information about the nature of the solution to eq (2). No characteristic can be periodic because, from (21), the value of R is strictly increasing,

so the characteristic path cannot loop around and return to a previous point. Since we have already established that the flow field has no critical points, the Poincaré-Bendixson Theorem implies that any characteristic passing through Q must exit through the boundary of Q as $s \to \infty$. By reversing the flow field, we also see from the Poincaré-Bendixson Theorem that any characteristic passing through Q must enter through the boundary of Q as well. In other words, every point in Q is connected to a characteristic that must enter and must exit through the boundary in Q — no characteristic remains in the interior of Q as $s \to \pm\infty$. Therefore knowledge of u, u_r, and u_y at all the boundary points of Q leads to knowledge of u throughout Q. We are interested, however, in the minimal amount of knowledge necessary to solve eq (2). If we assume the boundary of Q is piecewise smooth, knowledge of u on the boundary can be combined with the known intensity function, I, and the assumption that u_y and u_r are continuous and $u_r > 0$ to determine the values of u_r and u_y on the boundary. Further, we only need knowledge at one point on each characteristic, not two points, so knowledge of u at all the points of the boundary of Q where trajectories enter Q will be sufficient to determine u throughout Q. We must know u at each of these entrance points or else we will be unable to solve for u along the characteristic associated with the unknown entrance point. Technically, this means that the minimal amount of information needed to solve eq (2) is the value of u along a dense subset of the subsection of the boundary of Q associated with trajectories immediately entering Q. Realistically, we look for the value of u along all parts of the boundary of Q that could possibly be associated with trajectories entering the region Q.

As an example that we will use for the remainder of this paper, we consider the case where Q is the following rectangle in the (r, y) plane:

$$Q \equiv \{(r, y) : r \in [R_0, R_1] \quad y \in [Y_0, Y_1]\},$$

where R_0, R_1, Y_0, and Y_1 are constants. From (21) we know that along the line $r = R_0$, characteristics must enter Q, and along $r = R_1$, they must exit Q. Characteristics may enter or exit along the other two boundaries (see fig. 5). Therefore, if we know the value of u along $r = R_0$, $y = Y_0$, and $y = Y_1$, we are guaranteed to have enough information to solve eq (2).

From (21) we see that information always propagates in the direction of increasing r, which suggests that the tangent line to any characteristic at any point can never be parallel to the y axis. (This can be easily proven using eq (21), eq (20) and the physical restriction that both I and u_y must stay finite; we will further extend this restriction on the characteristic slopes in the CFL analysis of the next section.) Because the characteristic slopes are never parallel to the y axis, we never propagate information in a direction perpendicular to any characteristic if we numerically solve eq (2) by working in the direction of increasing r. Therefore Wildey's concern over propagating information in a direction perpendicular to a characteristic never materializes. Wildey's other concern was the instability of his numerical scheme for solving the SAR SFS problem. We present a stable scheme for solving eq (2) in the next section.

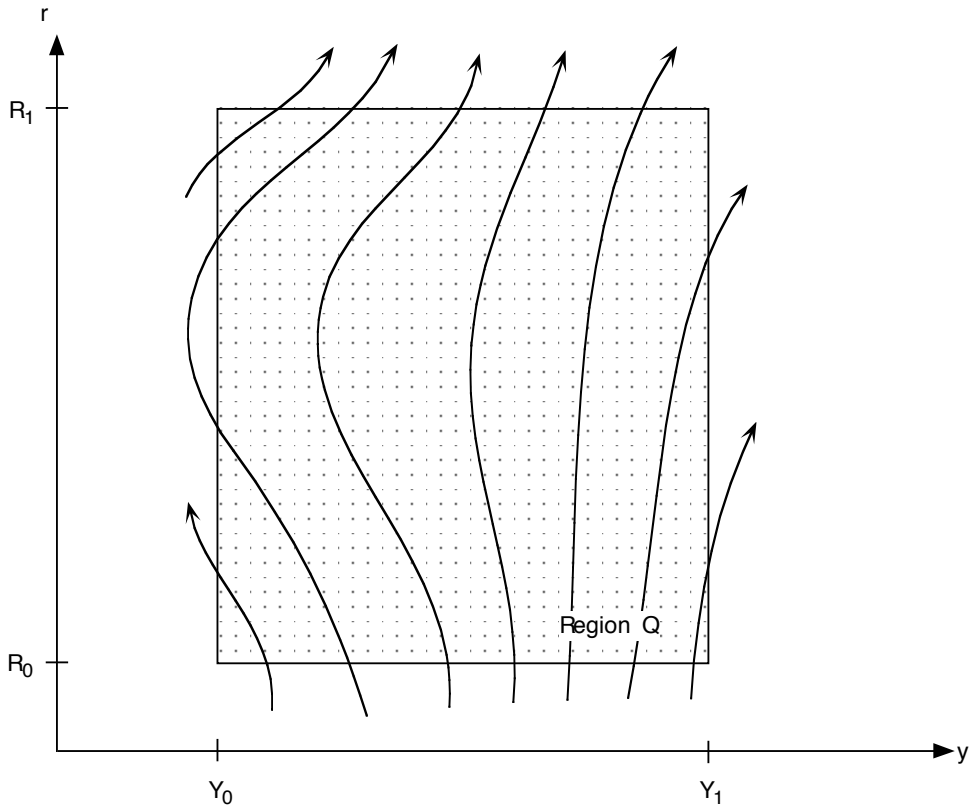

Figure 5: *Characteristic curves for Synthetic Aperture Radar Shape From Shading. Notice that the characteristics always progress in the direction of increasing* r.

5 Numerical Algorithms for Synthetic Aperture Radar

Because information always propagates in the direction of increasing r, we can make a useful comparison between SAR SFS and time dependent physical phenomena, where information always propagates in the direction of increasing time, t. We wish to exploit the vast numerical (and theoretical) knowledge that exists for equations of the form

$$\frac{\partial U(x,t)}{\partial t} + f\left(t, x, \frac{\partial U(x,t)}{\partial x}\right) = 0. \tag{22}$$

Equations of this type are called *time-dependent Hamilton-Jacobi* equations. In equations of this form, s, the parameter specifying location on a characteristic, equals t. So, in essence, converting to this form normalizes the parameterization of the characteristics so that a fixed change in s corresponds to the same fixed change in the coordinate direction in which information propagates. Specifically, we can rearrange eq (2) to algebraically isolate u_r, which yields eq (2)'s Hamilton-Jacobi form:

$$u_r - I\sqrt{.5 + \sqrt{.25 + (1 + u_y^2)/I^2}} = 0. \tag{23}$$

Recent finite difference methods can be applied to equations of this form. We will use the finite difference numerical algorithm developed by Osher and Shu [26] in this paper.

Before we look at the results of the algorithm, we wish to note some important advantages and generalizations of this method:

1) This analysis can also be applied to the non-Lambertian SAR case modelled by eq (3). Application of eq (15) to eq (3) reveals characteristics that imply a propagation of information in the r direction, just as in the Lambertian case. From the Implicit Function Theorem, we know that we can algebraically isolate u_r and obtain the Hamilton-Jacobi form of eq (3). In the interests of simplicity, however, we will continue to focus on eq (2) instead of eq (3).

2) We choose finite difference methods over existing control theory based methods of numerically simulating these equations since control theory methods require repeated iteration to converge to the value of the solution, whereas finite difference methods compute the solution value directly, which can save computational time.

3) Although we have restricted ourselves to smooth C^2 surfaces in this paper, any monotone numerical finite difference scheme will also construct a stable (viscosity) solution to eq (2) (or eq (3)) for any non-smooth (but continuous) surface given appropriate boundary conditions when the intensity is continuous. This can be extended to cases where the intensity data is discontinuous. A discussion of when uniqueness can be established for discontinuous intensity data and a proof that if uniqueness is established, any monotone numerical scheme will reconstruct this unique surface can be found in [27]. Mathematically, surface ridges occur when different characteristic curves cross. Much of the computational time in the Osher-Shu

essentially non-oscillatory (ENO) algorithm is devoted to constructing the viscosity solution when the characteristics cross, so more simple algorithms that are significantly faster than what we have used in this paper can be applied if we know that the solution is smooth (i.e., that the characteristic curves never cross).

Before applying the Osher-Shu algorithm, we must consider the CFL (Courant, Friedrichs, and Lewy) stability condition for eq (23). This condition is a restriction on the ratio of the "time" step, Δr, to the "space" step, Δy, employed by the program. This stability restriction follows from an inability to compute the solution at the point $(r_i+\Delta r, y_j)$ if the characteristic curve that passes through this point crosses the line $r = r_i$ at a location outside of the range $[y_j - \Delta y, y_j + \Delta y]$. Specifically, if we write eq (23) in the form

$$u_r + g(I, u_y) = 0, \tag{24}$$

then $\frac{dY}{dr}$, the speed (i.e., inverse of the slope) of a characteristic in the (r, y) plane, is determined from eq (15) to be

$$\frac{dY}{dr} = \frac{\partial g}{\partial u_y} = \frac{-u_y}{2I}\left[\left(\frac{1}{2} + \left(\frac{1}{4} + \frac{1+u_y^2}{I^2}\right)^{\frac{1}{2}}\right)\left(\frac{1}{4} + \frac{1+u_y^2}{I^2}\right)\right]^{-\frac{1}{2}}, \tag{25}$$

and the CFL condition requires that

$$\left|\frac{\partial g}{\partial u_y}\right| \frac{\Delta r}{\Delta y} \leq 1. \tag{26}$$

It is straightforward to show from eq (25) that the magnitude of the characteristic speed must always be less than $\frac{1}{2}$, therefore the CFL condition is satisfied if

$$\frac{\Delta r}{\Delta y} \leq 2. \tag{27}$$

We now consider the example of a rectangular region $\{(r, y) : r \in [0, 4] \text{ and } y \in [0, 4]\}$ with $\Delta r = \Delta y = 0.1$ where the intensity function on the region (see fig. 6) corresponds to u values for a tilted plane with a large indentation at $(2, 2)$ and a smaller indentation at $(1, 1)$. (Note that we have translated r so that $r = 0$ now represents the distance R_0 from the satellite.) When the numerical algorithm for eq (23) was fed the intensity function, $I(r, y)$, and the value of u along $y = 0$, $y = 4$, and $r = 0$, it reconstructed the 40 by 40 pixel representation of the original dented plane (shown in fig. 7) almost instantly on a Power Macintosh 9500/132. The computer reconstructed a 200 by 200 pixel representation of the surface in four seconds.

Since we are interested in viewing the surface in standard Cartesian coordinates we must rotate the reconstruction. Since φ, the angle of the radar signal, is essentially constant and the variation in r over the surface is small compared to the distance between the satellite and the surface, we may transform the (r, y, u) coordinates of the reconstruction into their

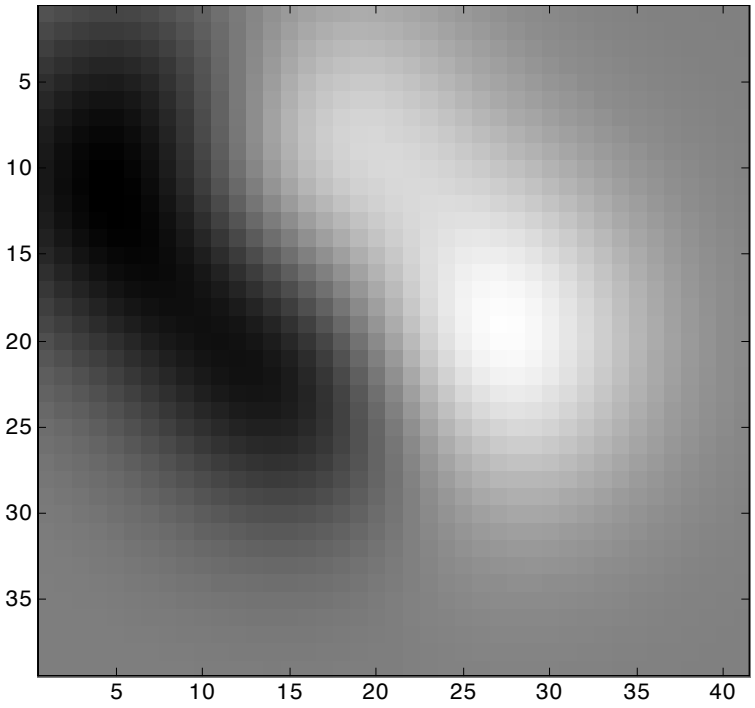

Figure 6: *Intensity data for a plane with two dents. Both the (horizontal) r axis and the (vertical) y axis are divided into 40 segments (each of which corresponds to length 0.1). The lighter regions of the picture represent higher values for the returned intensity.*

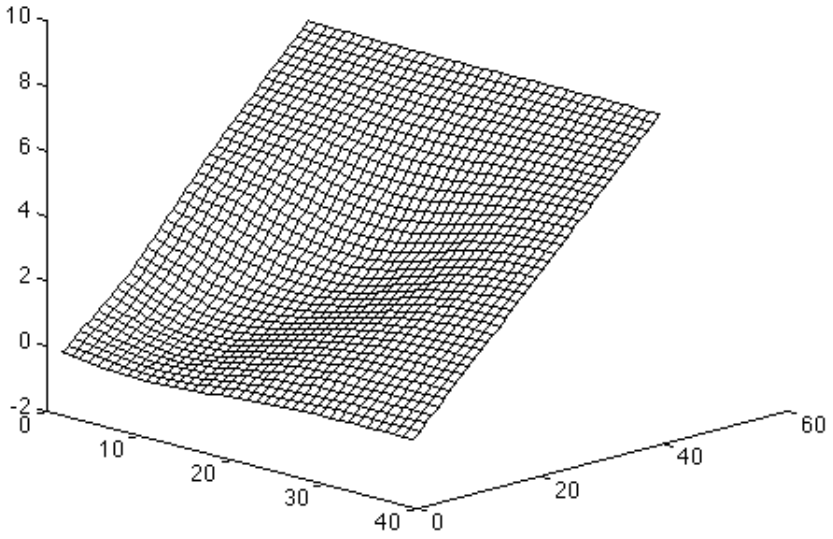

Figure 7: *Numerically reconstructed values for $u(r, y)$. u is the height. y is the axis that moves out of the page. r is the axis moving into the page. Notice that u_r remains positive.*

corresponding Cartesian coordinates (x, y, z) using the following rotation matrix transformation:

$$\begin{pmatrix} x \\ y \\ z \end{pmatrix} = \begin{pmatrix} \cos\left(\frac{\pi}{2} - \varphi\right) & 0 & \sin\left(\frac{\pi}{2} - \varphi\right) \\ 0 & 1 & 0 \\ -\sin\left(\frac{\pi}{2} - \varphi\right) & 0 & \cos\left(\frac{\pi}{2} - \varphi\right) \end{pmatrix} \begin{pmatrix} r \\ y \\ u \end{pmatrix}. \tag{28}$$

(Note that we use x and y here to represent the coordinates parallel to the surface and z to represent the height above the surface. This should not be confused with the x, y, z definitions used in the flat surface approximation where the x and z coordinates were rotated.) The rotation transformation results in the Cartesian view of the surface shown in fig. 8.

By considering only the (x, y) coordinates of the Cartesian reconstruction (see fig. 9), we can gauge the effect of the "flat surface" approximation in eq (9). If this approximation had been employed, the (x, y) coordinates would have been distorted to conform to a rigid square grid, as opposed to the appropriate wavy grid exhibited in fig. 9.

While we have shown that surface reconstructions with SAR radar data are nonunique if boundary conditions are not specified, we have not yet discussed the smoothness of the reconstructed surface. If we assume that the surface is smooth, we can remove from consideration potential boundary conditions that lead to reconstructions with discontinuities in the surface gradient (which occurs when characteristic curves intersect). This leads to the question of whether a smooth surface only has one boundary condition that will lead

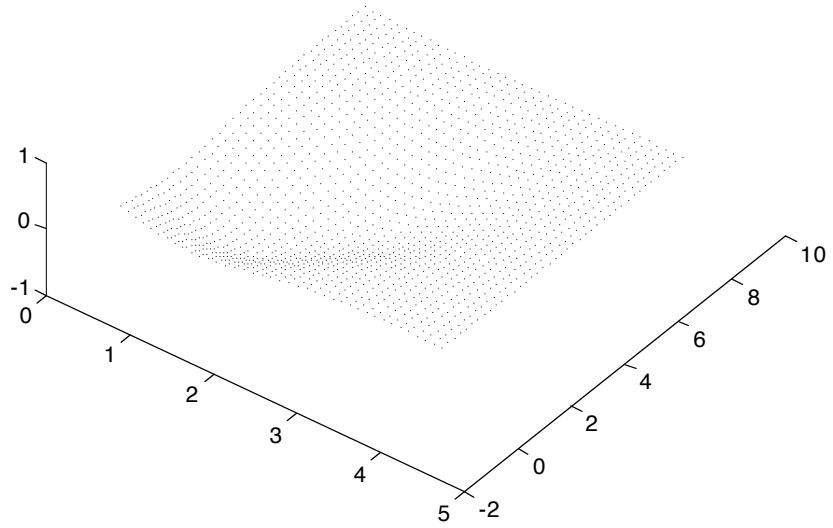

Figure 8: *Rotated Cartesian reconstruction. The y axis moves out of the page. The x axis moves into the page. The original dented surface is now clear.*

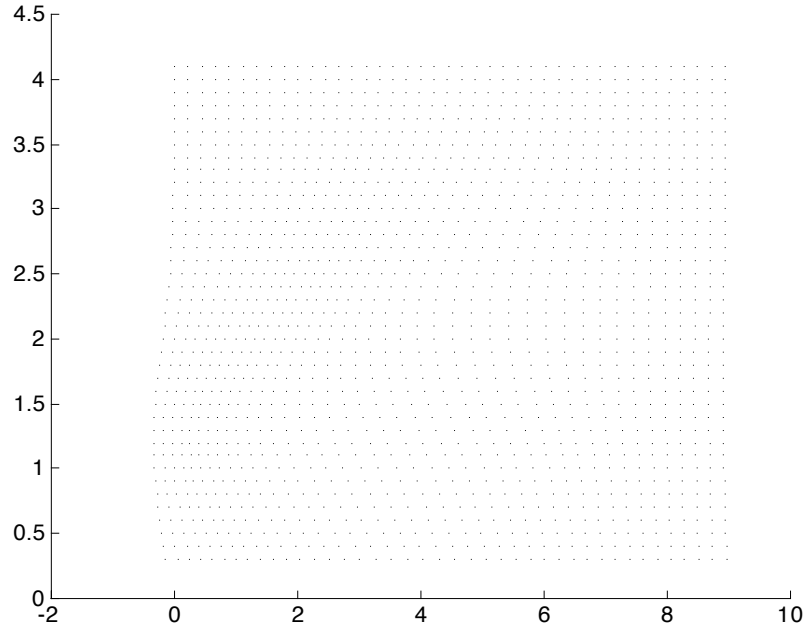

Figure 9: *View of the dented surface from above. The wavy nature of the* (x, y) *coordinates for the points of the surface reconstruction are appropriate. Standard "flat surface" approximations distort these coordinates so that the wavy nature is artificially removed.*

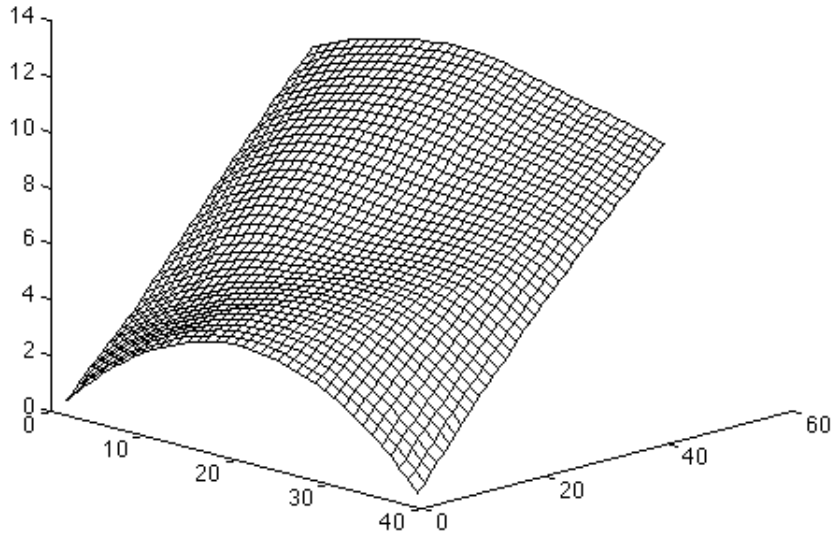

Figure 10: *Alternative $u(r, y)$ reconstruction from the intensity data in Figure 6.*

to a smooth reconstruction. If this were true, knowledge that the surface is smooth would allow us to recover uniqueness in the reconstruction. Unfortunately, this is not true; there are numerous counter-examples where (at least) two boundary conditions lead to solutions whose characteristics do not intersect, yielding a smooth surface reconstruction.

For example, we again consider the intensity data shown in fig. 6. As opposed to the almost flat condition given at R_0 to reconstruct the surface in fig. 7, we consider a parabolic condition at $R = 0$, which leads to the smooth reconstruction of $u(r, y)$ given in fig. 10.

This corresponds to the Cartesian representation of the surface produced in fig. 11.

It is clear that fig. 8 and fig. 11 are significantly different surfaces, yet both are smooth Cartesian reconstructions that are fully consistent with the intensity data given in fig. 6, demonstrating the nonuniqueness of SAR reconstructions when boundary conditions are not specified.

This, of course, leads to the practical question of determining boundary conditions so that a unique reconstruction can be ascertained. If exact data is not readily available, one can often rely on physical common sense to determine appropriate boundary conditions. For example, one of the typical uses of the data from Magellan has been to analyze volcanos found on the Venusian surface. These volcanos, however, are often surrounded by flat surface regions. Although flat regions create SAR data that correspond to *any* plane where the dot product of the unit surface normal with the unit normal in the direction of the radar signal equals $\cos(\varphi)$, we, of course, wish to select the unique plane that is tangent to the spherical

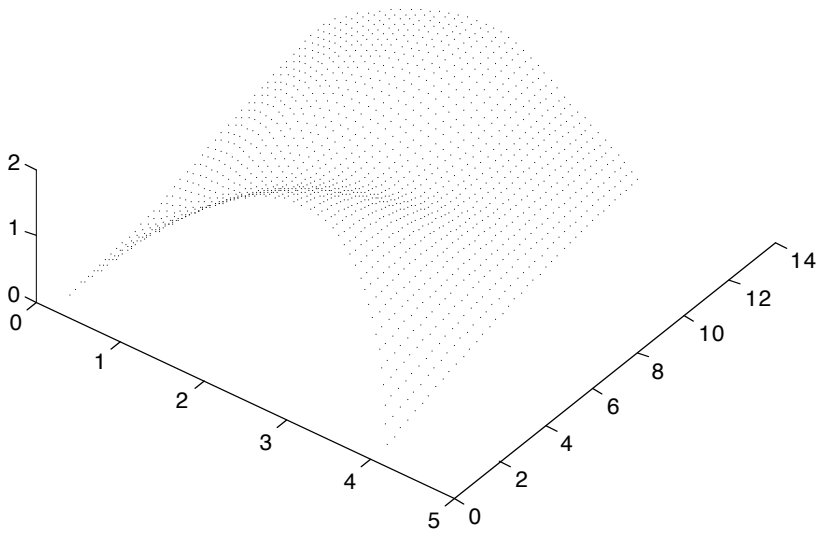

Figure 11: *Cartesian rotation of $u(r, y)$ data expressed in Figure 10. Both the surface presented here and the surface in Figure 8 are smooth and fully compatible with the intensity data in Figure 6.*

surface of the planet, which yields boundary conditions for the flat region surrounding the volcano, which can then be used to properly reconstruct the volcano. In the case of Magellan data, one could also attempt to utilize Magellan's low resolution altimetry data, although this would only provide a crude approximation of both the surface and the boundary conditions and would certainly lead to inaccuracies. (In Magellan's SAR data, each pixel corresponds to approximately 225 m x 225 m, whereas the Magellan altimetry data only determines the average surface height for 5 km x 5 km pixels called "footprints".)

Even when the height along three sides of a rectangle are not known, useful conclusions can still be ascertained if we know just the height at $r = 0$. Because we know that the magnitude of the characteristic speed $\left|\frac{dY}{dr}\right|$ must always be greater than $\frac{1}{2}$, we can place arbitrary conditions at $y = Y_0$ and $y = Y_1$ and then discount the results that could possibly be influenced by these fictional y boundaries. The potential domain of influence of these conditions — where the results should be ignored — is

$$\{(r, y) : r > 2(y - Y_0) \text{ or } r > -2(y - Y_1)\},$$

but the remaining isosceles triangular region of the (r, y) plane can be influenced only by characteristics emanating from the line $r = 0$, where the boundary conditions are known, and therefore the results of the reconstruction are accurate in this region (see fig 12).

Finally, if for some physical reason we know that u_y is negative or zero when $y = Y_1$, then it follows from eq (25) that characteristics cannot enter region Q through the line $y = Y_1$,

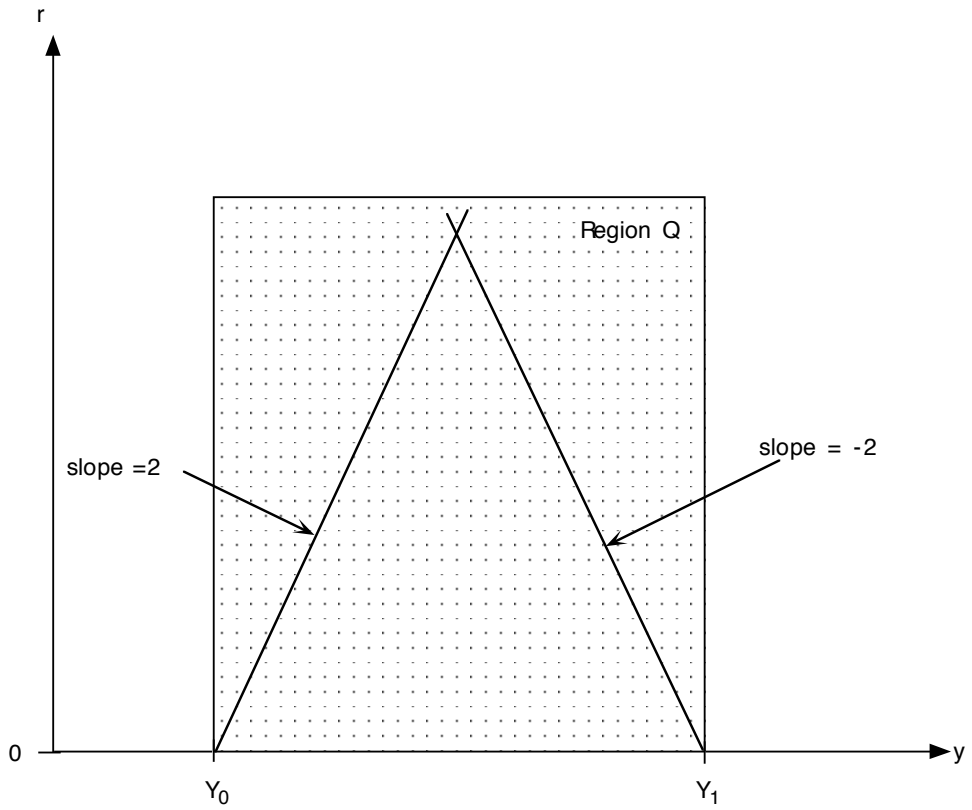

Figure 12: *Reconstructions from only one known line of boundary conditions. If the surface height is known along $r = 0$ between $y = Y_0$ and $y = Y_1$ then the surface can be reconstructed for all points inside the pictured triangle.*

and therefore there is no need to specify accurate boundary conditions at $y = Y_1$. Similarly if we have a priori knowledge that u_y is positive or zero when $y = Y_0$, then there is no need to determine boundary conditions along the line $y = Y_0$.

6 The Effect of Noise on the Intensity Data

Any set of SAR intensity data will be corrupted by noise. The complex-valued radar signal sent from the satellite is affected by the numerous facets and imperfections (speckle) of the surface. The Central Limit Theorem implies that these surface irregularities will induce an approximately Gaussian distribution in both the real and imaginary components of the signal returned to the satellite. Since the intensity (or power) of the returned signal is the square of the magnitude of the complex-valued radar signal, the intensity value produced from one radar signal will have a Chi-squared distribution with 2 degrees of freedom.

Typical intensity data, however, is not generally produced from a single returned signal. Instead each surface pixel is checked many times during SAR data collection. The number of times the radar sends a signal to each surface pixel is called the number of *looks* given by the satellite. The final intensity data is produced by averaging the intensities of each of the individual signals (i.e., incoherent averaging). This leads to a distribution in the intensities governed by

$$I_{\text{observed}}(r, y) = (I_{\text{noiseless}}(r, y))\frac{\chi^2_{2n}(r, y)}{2n}. \tag{29}$$

where n is the number of looks the satellite gives to each pixel, and χ^2_{2n} is a chi-squared random variable with $2n$ degrees of freedom. (The intensity can also be corrupted by thermal noise and the inability of signal processing to completely remove the effects of neighboring pixels. However, if the magnitude of the thermal noise is known, its effect can be removed from the final intensity data, and the "bleedthrough" from neighboring pixels is often negligible in practice, therefore we do not consider the effect of either in eq (29).)

To show the effect of noise on a surface reconstruction, we consider a 50 y-value by 75 r-value pixel reconstruction of a surface, $u(r, y)$, created from intensity data uncorrupted by noise (see fig. 13):

Since the effective number of looks of the Magellan satellite was usually between 20 and 40, we compute the reconstruction of $u(r, y)$ obtained from intensity data corrupted by 40 look noise (fig. 14), 20 look noise (fig. 15), and — for comparison — the worst case, 1 look noise (fig. 16).

One can clearly see the detrimental effect that reducing the number of looks has on the reconstruction.

As with any evolution based method, the reconstruction becomes worse as r increases and the effect of the noise accumulates. This is not necessarily a bad thing, however, as it indicates the quality of the intensity data. As stated earlier, cost minimization based techniques are often employed for particularly noisy data since they tend to encourage nicely

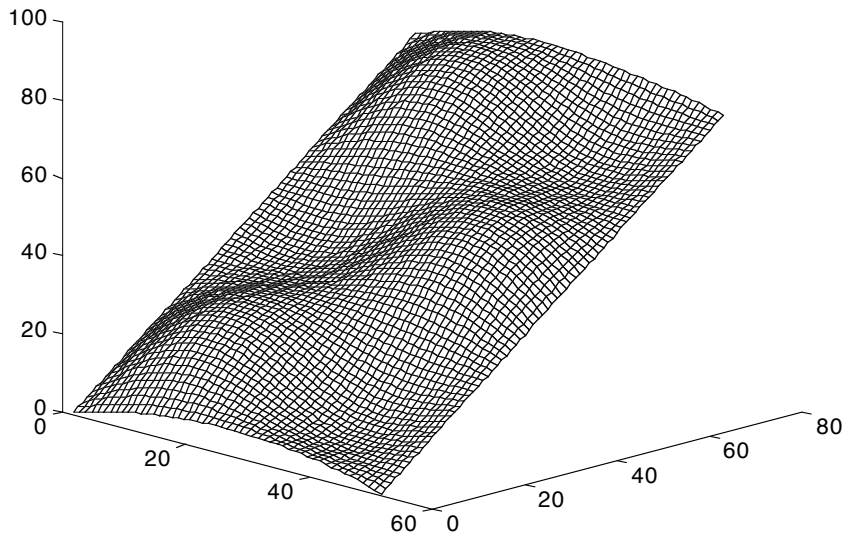

Figure 13: *Reconstructed $u(r, y)$ surface from intensity data uncorrupted by noise.*

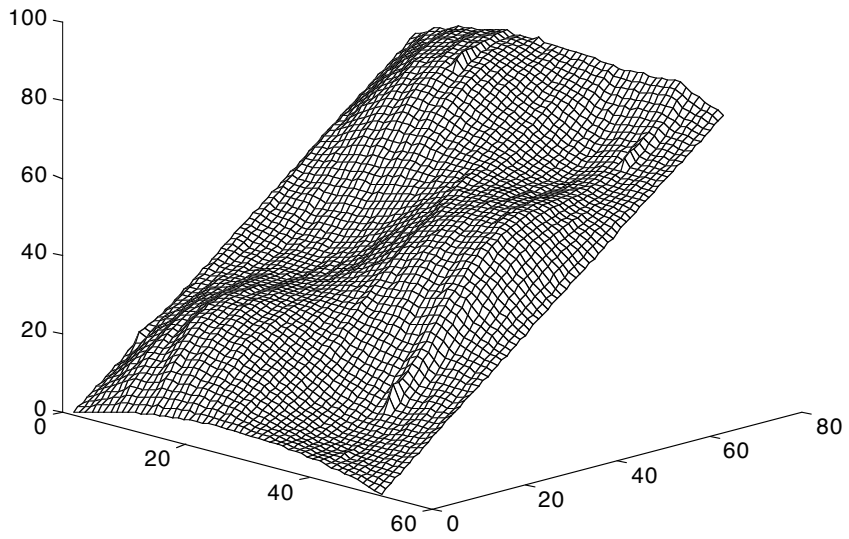

Figure 14: *Reconstructed $u(r, y)$ surface from intensity data corrupted by 40 look noise.*

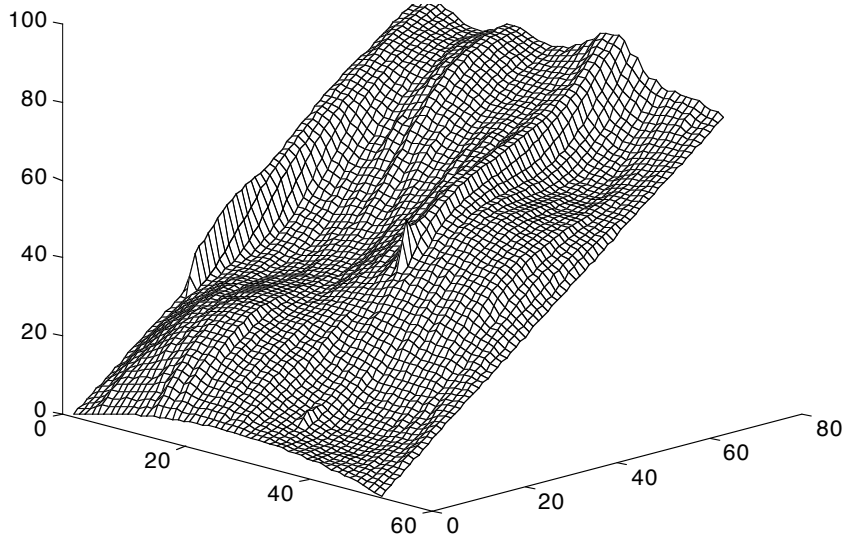

Figure 15: *Reconstructed $u(r, y)$ surface from intensity data corrupted by 20 look noise.*

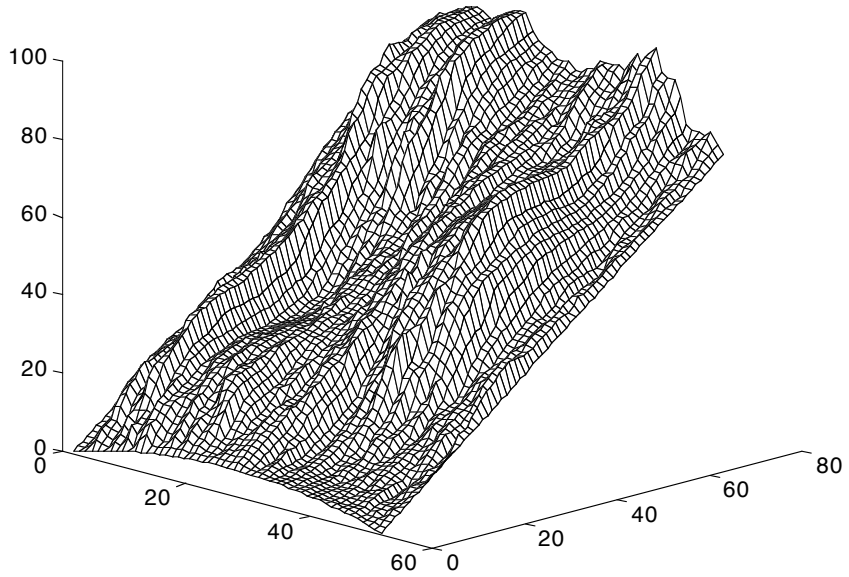

Figure 16: *Reconstructed $u(r, y)$ surface from intensity data corrupted by 1 look noise.*

behaved, smoother surfaces. This creates a potential danger since the surfaces will always appear satisfying — even when they are obtained from intensity data that may, in reality, be too noisy for meaningful reconstructions.

For SAR data with little or no noise, the partial differential equation approach presented here has clear advantages both in terms of clarifying the necessary boundary conditions and in terms of the speed of computing the solution. For noisy data, the numerical partial differential equation approach to SAR reconstructions can be helpful to cost minimization schemes in three ways: 1) It can quickly suggest when the intensity data is too noisy to be useful, 2) It can approximate even noisy solutions quickly, which can be used to generate a good starting point for the slower iterative cost minimization algorithms, saving computational time and reducing the likelihood that the cost minimization algorithm will tend toward an inaccurate surface corresponding to a local, but not global, cost minimum, 3) It suggests which boundary conditions should be incorporated into the cost minimization functional so that surfaces corresponding to false boundary conditions are discouraged.

Acknowledgments: I would like to thank Paul Dupuis and Stuart Geman for numerous useful discussions throughout the intial stages of this work, and Don McClure and Chi-Wang Shu for additional helpful suggestions. I would also like to acknowledge the financial support of the U.S. Army Research Office (Grant No. DAAL03-92-G-0115) and ARPA (Contract No. MDA972-93-1-0012) during some of the initial work on this paper.

References

[1] G. H. Pettengill et al., Magellan: Radar Performance and Data Products, *Science*, Vol. **252**, April 12, 1991, pp. 260–270.

[2] J. van Diggelen, A Photometric Investigation of the Slopes and the Heights of the Ranges of Hills in the Maria of the Moon, *Bull. Astron. Inst. Netherlands*, Vol. **11**, no. 243, 1951, pp. 283–290.

[3] T. Rindfleish, Photometric Method for Lunar Topography, *Photogrammetric Engineering*, Vol.**32**, no. 2, 1966, pp. 262–277.

[4] K. Watson, Photoclinometry from Spacecraft Images, *U.S. Geological Survey Professional Paper 599B*, 1968, p.1-B10.

[5] R. L. Wildey, Radarclinometry for the Venus Radar Mapper, *Photogrammetric Engineering And Remote Sensing*, Vol.**52**, no. 1, 1986, pp. 41–50.

[6] B. K. P. Horn, Obtaining Shapes from Shading Information, in *Psychology of Computer Vision*, McGraw-Hill, New York, 1975, pp. 115–155.

[7] R. L. Wildey, The Surface Integral Approach to Radar Clinometry, *Earth, Moon, and Planets*, Vol.**41**, 1988, pp. 141–153.

[8] M.J. Brooks and B. K. P. Horn, Shape and Source From Shading Information, in *Proceedings IJCAI-85*, Los Angeles, CA, 1985, pp. 932–936.

[9] K. Ikeuchi and B. K. P. Horn, Numerical Shape from Shading and Occluding Boundaries *Artificial Intelligence*, Vol.**17**, 1981, pp. 141–184.

[10] B. K. P. Horn and M. J. Brooks (eds.), *Shape From Shading*, MIT Press, Cambridge, 1989.

[11] R. T. Frankot and R. Chellappa, A Method for Enforcing Integrability in Shape From Shading algorithms, *IEEE Trans. Pattern Anal. Machine Intell.*, Vol.**10**, 1988, pp. 439–451.

[12] Q. Zheng and R. Chellappa, Estimation of Illuminant Direction, Albedo, and Shape From Shading, *IEEE Trans. Pattern Anal. Machine Intell.*, Vol. **13**, July 1991, pp. 680–702.

[13] T. Simchony, R. Chellappa, and M. Shao, Direct Analytical Methods for Solving Poisson Equations In Computer Vision Problems, *IEEE Trans. Pattern Anal. Machine Intell.*, Vol. **12**, May 1990, pp. 435–446.

[14] M. Shao, T. Simchony, and R. Chellappa, *Proc. CVPR*, June 1988, pp. 530–535.

[15] R. T. Frankot and R. Chellappa, Application of a Shape From Shading Technique to Synthetic Aperture Radar Imagery, *IEEE Int. Geosci. Remote Sensing Symp. (Ann Arbor)*, 1987, pp. 1323–1329.

[16] R. T. Frankot and R. Chellappa, Estimation of Surface Topography from SAR Imagery Using Shape From Shading Techniques, *Artificial Intelligence*, Vol.**43**, 1990, pp. 271–310.

[17] F. W. Leberl, *Radargrammetric Image Processing*, Artech House, 1990.

[18] K. D. Hartt, *Bayesian Estimation of Surface Information from Radar Images*, Ph.D. Thesis, University of Massachusetts-Amherst, 1993.

[19] A. R. Bruss, The Eikonal Equation: Some Results Applicable to Computer Vision, *J. Math. Phys.*, Vol.**23**, 1982, pp. 890–896.

[20] B. V. H. Saxberg, *Int. J. Robot. Res.*, Vol. **11**, No. 3, June 1992, pp. 202–224.

[21] P. Dupuis and J. Oliensis, An Optimal Control Formulation and Related Numerical Methods for a Problem in Shape Reconstruction, *Annals of Applied Probability*, Vol. **4**, 1993, pp. 287–345.

[22] J. Oliensis, Shape From Shading as a Partially Well-Constrained Problem, *Comput. Vision, Graphics, Image Process.: Image Understanding*, Vol.**54**, 1991, pp. 163–183.

[23] J. Oliensis, Uniqueness in Shape From Shading, *Int J. Comput. Vision*, Vol.**6**, 1991, pp. 75–104.

[24] M. Eastwood, Some Remarks on Shape from Shading, *Advances in Applied Mathematics*, Vol. **16**, 1995, pp. 259–268.

[25] N. E. Hurt, Mathematical Methods in Shape-from-Shading: A Review of Recent Results, *Acta Applicandae Mathematicae*, Vol.**23**, 1991, pp. 163–188.

[26] S. Osher and C. Shu, High-Order Essentially Nonoscillatory Schemes for Hamilton-Jacobi Equations, *SIAM J. Numer. Anal.*, Vol.**28**, No. 4, August 1991, pp. 907–922.

[27] D. Ostrov, Viscosity Solutions and Convergence of Monotone Schemes for Synthetic Aperture Radar Shape-From-Shading Equations with Discontinuous Intensities, (to appear)